Volume 17, Issue 1, 172506 (1-14)

Iranian Journal of Earth Science (IJES)

https://dx.doi.org/10.57647/j.ijes.2025.1701.06

Geochemical characteristics of hydrothermal manganese deposits in the Sulaimani metallogenic district, Kurdistan Region of Iraq: A serpentinization marker

Dnya Abdalwahab Latif[1], Yousif Osman Mohammad[1]*, Mushir Mustafa Qadir[1], Hossein Azizi[2]

[1]*Department of Earth Sciences and Petroleum, College of Science, University of Sulaimani, Sulaymaniyah, Iraq.*
[2]*Department of Mining Engineering, Faculty of Engineering, University of Kurdistan, Sanandaj, Iran.*

*Corresponding author: yousif.mohammad@univsul.edu.iq

Original Research Paper

Received:
7 March 2024
Revised:
10 June 2024
Accepted:
13 July 2024
Published online:
10 January 2025

Abstract:

This research investigates the geochemical characteristics of hydrothermal manganese deposits in the Sulaimani metallogenic district, Kurdistan Region of Iraq, to understand their formation processes, which may aid in the exploration of manganese resources in the region. These deposits are intimately associated with various units of Mesozoic Qulqula Formation, including jasparite, umber, radiolarian chert, siliceous shale, brown claystone, and basalt sequences of the Penjween ophiolite in the Mlakawa - Tapa sura area. In the Sulaimani district, two types of manganese deposits are found: strata-bound deposits with a thickness of around 200 meters, interbedded with late Cretaceous eip-ophilitic radiolarite chert of the Penjween ophiolite complex, and as exotic massive bodies within Eocene Merga Group, forming boulder placer deposits. The manganese deposits exhibit geochemical characteristics such as intermediate MnO content (up to 24 wt.%), low levels of transitional elements (Co + Ni + Cu $<$ 0.01 wt.%), elevated concentrations of Ba (up to 4490 ppm), and low total rare earth elements. Geochemical analyses reveal negative Ce anomalies (-0.016 _ -1.024) and positive Y anomalies (3.4 _ 22.3) in most samples, indicative of submarine hydrothermal processes within the Neotethys. However, some banded-type deposits show weak positive Ce anomalies (0.1), suggesting minor diagenetic influences. The presence of weak negative Eu anomalies (0.54 _ 0.71) in all samples likely reflects the low Eu content in the ultramafic parent rocks and the influence of low-temperature hydrothermal serpentinization fluids. In summary, the geochemical signatures suggest that these manganese deposits, associated with regional radiolarite facies within the Neotethys, originate from mid-oceanic ridge proximal to distal hydrothermal sources.

Keywords: Manganese deposits; Neotethys; Banded chert; Zagros orogeny; Sulaimani

1. Introduction

The significant and extensive Zagros Mountain belt in the Kurdistan region of Iraq emerged from the continental break off the Sanandaj–Sirjan Zone (SaSZ) from the Northwest of Afro-Arabian plate margin and the subsequent accretion of Eurasia (Jassim and Goff, 2006). This was followed by Eocene amalgamation with Arabian plate (Ghasempour et al., 2014; Mohammad, 2020; Nutman et al., 2022). The time sequence of the tectonic evolution of Zagros collisional orogens typically involves three major tectonic events: (1) Permian crustal divergence, (2) Late Cretaceous convergence, and (3) Eocene collisional, each giving rise to distinct types of ore deposits in specific time and diverse geological settings. The timing and distribution of mineral deposits in various region of Iraq demonstrate a strong correlation with tectonic divisions. In the Kurdistan region of Iraq, significant mineral deposits are characterized by endogenic metallic mineralization from the Jurassic, Upper Cretaceous, and Paleogene periods. These are connected to hydrothermal, magmatic, sedimentary, and metamorphic processes associated with regional orogenic phases (Al-Bassam, 2013).
The Kurdistan region of Iraq can be divided into two main metallogenic zones based on the regional tectonic framework of the Zagros orogenic belt. These zones are the Imbricate Zone of the Western Zagros Fold-Thrust Belt and

the Bitlis-Sanandaj-Sirjan Zone (Fig. 1; compiled from (Al-Bassam, 1984; Jassim and Goff, 2006; Fouad, 2012; Mohammad et al., 2014; Al-Bassam, 2013; Dabiri et al., 2018; Mollai et al., 2021).The former zone encompasses three mineral belts i) Qulqula-Khwakurk Mn-Fe belt is composed of hydrothermal and diagenetic Mn-Fe deposits within the radiolarian chert of the Early Cretaceous part of the Qulqula Series; ii) Penjween-Walash Cr, Ni, Cu, Fe belt, it contains orthomagmatic Cr, Ni, Fe, Cu and contact metasomatic skarn Fe. This belt consists of the Qandil Series (Early Cretaceous), basic and ultrabasic Igneous ophiolite Complexes (Late Cretaceous), and volcano sedimentary units of Walash and Naopurdan Groups (Tertiary); iii) Tertiary Red Beds placer deposit belt of Mn and Fe (Buday and Jassim, 1984; Jassim and Goff, 2006; Al-Bassam, 2013; Mahdavi et al., 2015; Sissakian, 2018).

Conversely, the Bitlis-Sanandaj-Sirjan Zone (BSaSZ) exhibits a diverse array of ore deposits that were formed during the Mesozoic era, including orthomagmatic, metamorphic, and hydrothermal deposits. Within the BSaSZ of Iraq, there are two significant metallogenic belts known as the i) Shalair -Marabasta Zn, Pb, Fe belt in the southeast. This belt is characterized by Jurassic metamorphosed Zn, Pb, and pyrite strata-bound deposits, which occur in carbonate rocks of Triassic origin. ii) The Ora belt in the north west, which includes both low temperature hydrothermal Ba, Cu, Pb, Zn, and pyrite veins, as well as to Late Triassic -Late Cretaceous syngenetic strata-bound deposits of Zn and Pb, along with disseminated pyrite in massive carbonate rocks; Additionally, there are other deposits found in the region, such as Fe and Zn skarns, volcanogenic Cu and Fe mineralizations, and Cretaceous marble deposits.

Manganese deposits are known to come from various sources, characterized by differences in mineralogy, chemical composition, and tectonic context (Polgari et al., 2012). Marine manganese deposits are categorized as hydrogenous, diagenetic, hydrothermal, or biogenetic-bacterial (Oksuz, 2011; Polgari et al., 2012). Furthermore, Mosier and Page (1988) identified four types of manganese deposits based on their tectonic settings: Franciscan, Cuban, Olympic Peninsula, and Cyprus types.

The Zagros hydrothermal manganese and ferromanganese deposits are commonly associated with fragments of the Neotethys oceanic crust, which include radiolarian cherts and basaltic rocks forming the top crustal unite ophiolite sequences (Zarasvandi et al., 2016; Maghfouri et al., 2019; Aydogan, 2021; Ousta et al., 2024). The upper pelagic sedimentary facies of the Neotethys oceanic basin extended from southern Oman, through western Iran's Kermanshah region, passing by Qulqula in the Kurdistan region of Iraq, and ending with the Kocali basin in northern Turkey (Wever et al., 1988; Mohammad and Qaradaghi, 2016; Nazari et al., 2023). Many economically significant manganese and ferromanganese deposits have been documented in various locations in association with Neotethys radiolarite, such as Oman (AI Hammah Range - Wahrah Formation), Iran (Nasirabad and Abadeh, Gugher and Gushk, Tashk, Sorkhvand and Kamyaran deposits), Turkey Emir deposit (Sorgun-Yozgat deposit), Greece (Andros), and Cyprus (Troodos Massif) (Kickmaier and Peters, 1990; Ozturk, 1997; Maghfouri et al., 2019).

Manganese occurrences connected to the Qulqula-Khwakurk Mn-Fe belt in the Kurdistan region of Iraq have been recorded ((Latif et al., 2022) and references therein). However, specific geochemical signatures of the manganese deposits associated with the Neotethys ophiolite unit in the Kurdistan region of the Zagros orogeny have not been considered. Consequently, this study marks the first effort to precisely describe these deposits, conduct comprehensive geochemical investigations, and explore the geological settings of manganese occurrences in this region. Furthermore, utilizing available geochemical datasets of manganese deposits across the region, we propose a geodynamic model that may elucidate the origin of Neotethys manganese and ferromanganese in radiolarite chert.

2. Geological setting and mode of occurrences of manganese deposits

Narrow belts and sporadic units of manganese deposits are found within radiolarian chert and Red Bed series in the Imbricated Zone of the Kurdistan region in Iraq (Fig. 1). These deposits are situated in a continuous belt that stretches across the Sulaimani metallogenic province, running from the southeast to the northwest along the collision zone. The manganese deposits in the epi-ophiolitic rock are closely associated with jasparite, umber (Fig. 2), radiolarian chert, siliceous shale, brown claystone, and a basalt succession of Penjween ophiolite in the Mlakawa - Tapa sura area.

The chert sequences in the area mainly represent the bedded facies of Qulqula radiolarite, which were deposited during the middle Jurassic to early Late Cretaceous period in the Neotethys oceanic basin (Baziany, 2014). Most man-

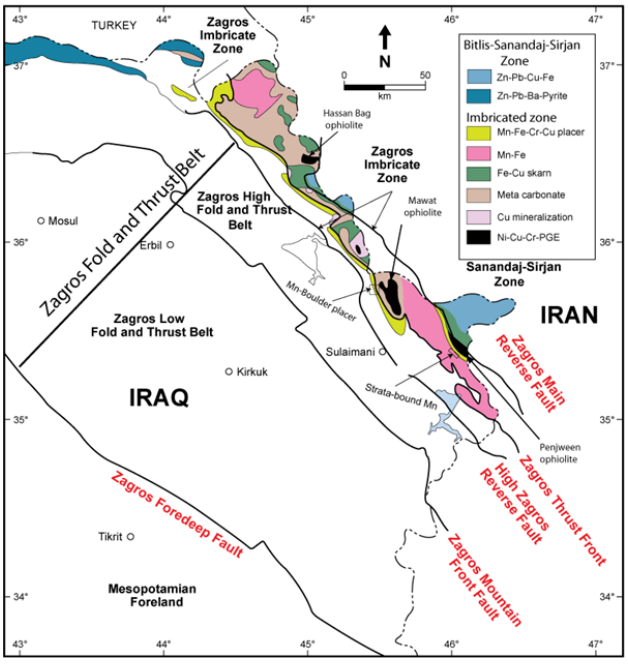

Figure 1. Tectono- mineralogenic map of Kurdistan region of Iraq, showing various mineral deposits belts superimposed on major tectonic zones (Tectonic subdivision from (Mohammad et al., 2014)).

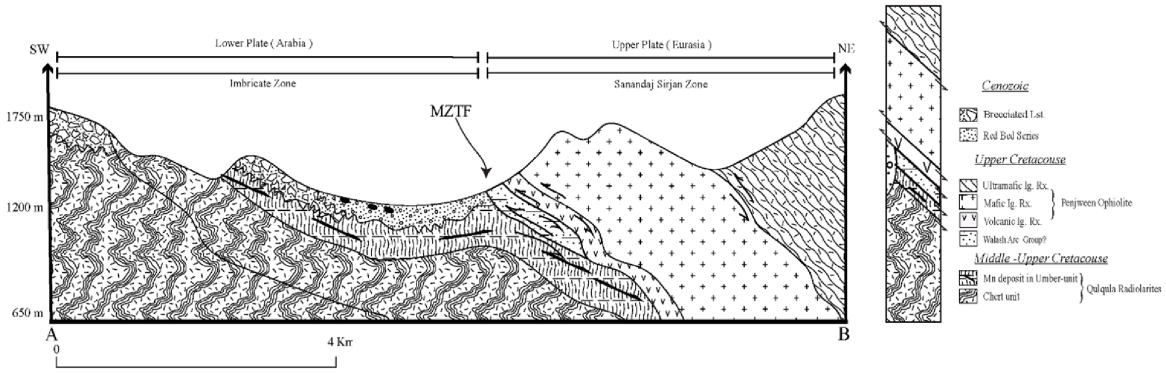

Figure 2. Geological cross section and stratigraphic column of Penjween area, showing the main lithostratigraphic units in addition to manganese occurrence.

ganese mineralization is typically found in close proximity to reddish-brown radiolarian cherts that overlie the volcanic unit of the Penjween ophiolite during the deposition process before final thrusting and emplacement stages of the Neotethys oceanic basin in the form of fossil fragment ophiolite (Fig. 2).

Penjween ophiolite consists of about 300 m thick mantle sequences mostly serpentinized harzburgite with some restricted dunite, pyroxenite veins and chromitite pods to the southwest, occupying the summit of Mlakawa mountain, to the west followed by about 2 Km crustal sequences represent by various types of gabbro, dykes of diorite and volcanic rocks at the Mlakawa mountain slope and base respectively (Mohammad et al., 2007; Mohammad, 2011; Mohammad et al., 2021; Yazdi et al., 2022). Within the volcanic units occasionally bolder and patches of metalliferous recrystallized quartz dominated rock occurs north of the Kani Manga village. The volcanic unit is underlined by umber unit then followed by typical chert unit of Qulqula Formation. As a result of the intense deformation, squeezing and extensive thrusting a combined obduction-collision event in the area it is obvious that the stratigraphy sequence of the Penjween ophiolite complex apparently overturned (Fig. 2). Field investigations have revealed the presence of various ore structures and sizes associated with radiolarian cherts, including layered, vein (2-5 cm thick veins), macronodular (1-3 cm across), and banded manganese (0.1 to 0.2 thick mm band) mineralization located approximately 5 kilometers southwest of Penjween ophiolite.

3. Mineralogy and mineral paragenetic

(Latif et al., 2022) based on detail ore microscopic investigations and XRD phase identifications confirmed that the mineralogy of manganese deposits in Sulaimani metallogenic province are relatively simple. The ore consists mainly of pyrolusite dominated with minor hollandite for the banded, vein and layer types of the ore, while massive types are braunite and rhodonite dominated. Quartz, cryptocrystalline silica, calcite, iron oxides and clay minerals are gangue minerals. Through sequences of layers in vain filling, replacement relationships among the manganese phases, recrystallization and deposition relative to the distal and proximal area of the discharging sources and subsequent metamorphism. Thus, it is evidenced from these relationships that the manganese deposit in the area may have formed through four successive stages as follow: Hydrothermal → Nano manganese deposition → Diagenetic → Metamorphic stages. Detail of mineralogy and paragenetic sequence described in (Latif et al., 2022).

4. Analytical methods

14 samples representing diverse manganese occurrences in the Sulaimani Metallogenic provinces have been selected for geochemical investigation through laboratory-based examination. The numbers of samples from manganese deposits chosen for geochemical analysis are illustrated in Table1. These include 3 samples from the massive type, 4 samples from the vein type, 5 samples from another vein type, and 2 samples from the host rock. Laboratory-based investigations included routine polarized transmitted-incident optical microscopy, complemented by Scanning Electron Microscope (SEM) and X-ray diffraction (XRD) studies. The microscopic examinations and XRD analysis were conducted at the Geology department of Sulaimani University, Kurdistan Region of Iraq. Detail results of mineral components and mineralogical description can be seen in (Latif et al., 2022).

The analysis for major, trace elements, and Rare Earth Elements (REE) in the whole-rock samples was carried at a certified lab (ALS Laboratory Group, SL), using ICP-AES with the Lithium Borate fusion method as part of the whole-rock package encoding ME-MS81d and ME-4ACD81. The QC/QA process involved analyzing duplicate samples (7% of the total samples), blanks, and certified reference materials (EMOG-17, MRGeo08). The concentration of major, trace, and REE in the samples given in Tables1 and 2. Additionally, the correlation coefficients between various oxides, trace elements, and REEs can be found in Appendix 1.

In this study, the RQ-mode PCA (Principal Component Analysis) method is used (Neff, 1994), which aids in conducting a more insightful analysis of the relationships between variables (elements) and observations (samples). By employing RQ-mode PCA, we can effectively examine and understand the interrelationships among variables and observations for the available geochemical dataset of manganese deposit in the study area. This approach may lead to a

Table 1. ICP-MS results of the major and trace element composition from various types of manganese deposits in the Sulaimani metallogenic province.

Sample No.	DY-1	DY-2	DY-3	DY-4	DY-5	DY-6	DY-7	DY-8	DY-9	DY-10	DY-11	DY-14	DY-12	DY-13
Major oxides (wt. %)	**Massive type**			**Chert**	**Vein type**				**Banded type**					**Jasperite**
Latitude (N)	***35°54′49″***			***35°30′00″***	***35°29′59″***				***35°30′41″***					***35°30′00″***
Longitude (E)	***45°23′82″***			***45°57′87″***	***45°58′01″***				***45°57′49″***					***45°57′87″***
SiO_2	63.6	68.3	65.6	96.3	69.7	79.3	64.6	71.7	83.5	77.7	76.6	86.8	86.7	91.1
Al_2O_3	0.54	0.31	0.55	0.76	1.23	1.14	1.9	1.8	2.34	2.4	1.78	2.55	0.09	0.49
TiO_2	0.03	0.01	0.03	0.03	0.06	0.05	0.11	0.1	0.13	0.14	0.11	0.14	0.01	<0.01
MgO	0.27	0.16	0.34	0.06	0.26	0.19	0.43	0.46	0.33	0.33	0.19	0.45	0.06	0.28
Fe_2O_3	14.2	15.9	8.64	0.53	0.91	0.59	1.03	1.08	1.5	1.35	1.16	1.4	4.01	7.83
CaO	3.63	2.69	4.76	0.7	1.6	0.21	0.52	0.49	0.25	0.23	0.16	0.39	0.07	0.05
Na_2O	0.04	0.02	0.02	0.13	0.1	0.13	0.16	0.15	0.12	0.11	0.11	0.12	0.03	0.02
K_2O	0.02	0.01	0.01	0.14	0.17	0.42	0.76	0.83	0.4	0.38	0.25	0.49	0.03	0.02
MnO	13	8.54	18.7	0.09	20.2	12.85	23.9	18.85	7.42	12.65	14.15	4.92	5.9	0.06
P_2O_5	0.08	0.05	0.1	0.06	0.07	0.04	0.09	0.07	0.03	0.04	0.02	0.12	0.03	0.03
SrO	0.01	0.01	0.01	0.01	0.01	0.02	0.02	0.02	0.01	<0.01	0.01	<0.01	0.01	<0.01
BaO	0.25	0.15	0.42	0.021	0.82	0.54	1.097	0.885	0.14	0.231	0.202	0.178	0.1	0.1
LOI	2.48	2.1	2.68	1.71	5.69	3.37	5.78	4.87	3.82	4.53	4.29	3.54	1.95	0.46
Trace elements (ppm)														
As	67	44	43	<5	8	<5	7	7	<5	<5	5	<5	48	6
Cr	20	20	10	40	20	50	70	60	10	10	10	20	20	30
Co	9	7	21	2	60	23	39	37	51	68	36	61	1	1
Ni	139	92	218	7	51	12	28	26	32	41	31	82	236	1
Cu	102	60	187	12	715	505	1030	822	57	122	135	35	22	7
Sc	1	<1	1	1	3	2	3	3	4	4	3	4	<1	<1
Zn	115	75	165	4	43	22	41	36	23	32	25	28	172	28
Sr	71.5	32.3	33.8	27.4	81.1	162	244	245	75.9	73.4	100	44.7	45.4	3.6
Ba	673	577	1355	178.5	635	2900	4210	4490	279	391	452	550	2000	8.6
Y	10.6	6.3	12	12.1	10.9	3.5	8.2	6.2	3.4	4.6	4.8	22.3	4.5	5.7
Zr	10	4	11	11	28	15	24	21	27	27	21	25	27	3
U	1.01	0.53	1.28	0.18	2.03	2.89	2.58	2.31	0.81	1.22	1.41	0.45	0.42	0.06
V	335	219	297	6	130	110	180	171	26	38	44	23	66	23
Hf	0.2	<0.1	0.2	0.3	0.4	0.3	0.5	0.5	0.6	0.6	0.5	0.6	0.1	0.1
Pb	26	18	33	5	96	24	36	29	19	25	23	11	11	7
Li	10	10	<10	20	20	20	20	20	20	20	20	30	<10	<10
Nb	0.6	0.2	0.6	0.8	2.8	2	3.1	2.9	2.5	3.3	2.3	0.3	0.1	2.9
Cs	0.01	0.01	0.01	0.14	0.32	0.22	0.46	0.43	0.62	0.71	0.44	0.02	0.02	0.72
Ta	<0.1	<0.1	<0.1	<0.1	<0.1	<0.1	0.1	<0.1	0.1	0.1	<0.1	<0.1	<0.1	0.1
Tb	0.2	0.09	0.22	0.35	0.23	0.09	0.21	0.15	0.09	0.15	0.11	0.06	0.14	0.56
Th	0.42	0.09	0.43	0.62	0.74	0.56	1.13	0.96	1.29	1.35	0.98	<0.05	<0.05	1.31
Rb	0.7	0.4	0.3	2.9	5.2	4.6	9.2	9	13.1	12.7	8.1	0.4	0.3	14.7
Hf	0.2	<0.1	0.2	0.3	0.4	0.3	0.5	0.5	0.6	0.6	0.5	0.1	0.1	0.6
Ga	8	5.3	11.7	1.5	11.4	8.1	13.5	10.6	6.3	8.6	8.8	3.4	2	5.5
W	1	1	1	<1	8	31	<1	<1	9	18	24	8	2	1
Cu+Co+Ni	250	159	426	21	826	540	1097	885	140	231	202	178	259	9
(Cu+Co+Ni)*10	2500	1590	4260	210	8260	5400	10970	8850	1400	2310	2020	1780	2590	90
Co/Zn	0.08	0.09	0.13	0.5	1.4	1.05	0.95	1.03	2.22	2.13	1.44	2.18	0.01	0.04
Mn/Fe	1.02	0.59	2.4	0.19	24.5	24.12	25.69	19.33	5.48	10.38	13.51	3.89	1.63	0.01
Th/U	0.42	0.17	0.34	3.44	0.36	0.19	0.44	0.42	1.59	1.11	0.7	0	0	2.91
Co/Ni	0.06	0.08	0.1	0.29	1.18	1.92	1.39	1.42	1.59	1.66	1.16	0	0	0.74

Table 2. ICP-MS results of the Rare Earth Element (REE) geochemical composition from various types of manganese deposits in the Sulaimani metallogenic province. * After (Taylor and McLennan, 1985)

Sample No.	DY-1	DY-2	DY-3	DY-4	DY-5	DY-6	DY-7	DY-8	DY-9	DY-10	DY-11	DY-14	DY-12	DY-13
REEs (ppm)	**Massive type**			**Chert**	**Vein type**				**Banded type**					**Jasperite**
La	6.7	3.4	9.2	10.1	14.6	4.3	9.5	7.1	4.2	5.9	3.7	21.2	2.1	0.7
Ce	3.6	1.4	3.5	12.2	15.5	8.5	16.9	12.7	11.7	16.5	10.9	20.3	0.4	1.9
Pr	1.28	0.54	1.73	2.82	2.14	0.84	1.85	1.4	0.9	1.4	0.99	4.67	0.34	0.32
Nd	5.2	2.1	7	11.4	7.6	3	6.9	5.1	3.1	5.1	3.7	18.8	1.3	1.8
Sm	1.13	0.41	1.34	2.43	1.5	0.6	1.43	1.04	0.65	1.07	0.81	3.68	0.32	0.55
Eu	0.27	0.11	0.35	0.57	0.37	0.14	0.32	0.22	0.14	0.26	0.18	0.91	0.06	0.12
Gd	1.33	0.56	1.59	2.58	1.68	0.6	1.36	1.11	0.6	0.99	0.78	4.14	0.36	0.84
Dy	1.32	0.67	1.47	2.02	1.58	0.54	1.23	0.97	0.58	0.85	0.64	3.19	0.37	0.94
Ho	0.3	0.16	0.32	0.39	0.34	0.11	0.24	0.19	0.11	0.16	0.13	0.63	0.09	0.2
Er	0.91	0.52	0.96	1.01	1.12	0.31	0.74	0.58	0.34	0.46	0.39	1.76	0.34	0.66
Tm	0.1	0.05	0.1	0.12	0.13	0.04	0.09	0.07	0.04	0.06	0.04	0.19	0.04	0.08
Yb	0.69	0.41	0.64	0.77	1.07	0.29	0.64	0.51	0.35	0.45	0.33	1.18	0.27	0.53
Lu	0.1	0.06	0.1	0.1	0.16	0.04	0.1	0.08	0.05	0.07	0.05	0.17	0.05	0.07
REE	22.93	10.39	28.3	46.51	47.79	19.31	41.3	31.07	22.76	33.27	22.64	80.82	6.04	8.71
LREE/HREE	5.7	4.55	6.88	9.54	9.86	13.51	12.58	11.94	14.48	15.22	13.32	10.35	4.2	2.51
La/Ce	1.86	2.42	2.62	0.82	0.94	0.5	0.56	0.55	0.358	0.35	0.33	1.04	5.25	0.368
Ce/Ce^*	0.28	0.24	0.2	0.53	0.64	1.04	0.94	0.94	1.41	1.34	1.33	0.47	0.11	0.94
Eu/Eu^*	0.67	0.7	0.73	0.69	0.71	0.71	0.7	0.62	0.68	0.77	0.69	0.71	0.54	0.53
La_N/Nd_N	2.49	3.13	2.54	1.71	3.72	2.77	2.66	2.69	2.62	2.24	1.93	2.18	3.12	0.75
Dy_N/Yb_N	1.24	1.06	1.49	1.7	0.96	1.21	1.25	1.23	1.078	1.22	1.26	1.75	0.89	1.15
Ce_{anom}	-0.58	-0.68	-0.7	-0.269	-0.268	-0.016	-0.064	-0.061	0.12	0.11	0.12	-0.348	-1.024	-0.027
Ce_{SN}/Ce_{SN^*}	0.28	0.23	0.2	0.52	0.62	1.02	0.92	0.92	1.38	1.32	1.31	0.11	0.87	0.47
Y_{SN}/Ho_{SN}	1.31	1.46	1.39	1.15	1.19	1.18	1.27	1.21	1.14	1.06	1.37	1.85	1.06	1.31
La_{SN}/Ce_{SN}	3.92	5.11	5.53	1.74	1.98	1.07	1.18	1.18	0.76	0.75	0.71	11.05	0.78	2.2

$Ce_{anom}=Log[3^* Ce_N/(2^* La_N+Nd_N)]^*$

$Ce^*=Ce_N/[2/3\ La_N+1/3\ Pr_N]^*$

$Eu^*=Eu_N/[2/3\ Sm_N+1/3\ Gd_N]^*$

deeper understanding of the geochemical characteristics of the manganese deposit and allows for the exploration of element associations, providing valuable insights into the geological processes and factors influencing the deposit's formation.

5. Results

The SiO_2 concentration varies from 63.6 to 96.3 wt.%, with an average of 77.25 wt. %, and CaO from 0.07 to 4.76 wt. %, with an average of 1.12 wt. % (Table1). The samples have a low Al_2O_3 content, ranging from 0.54% to 2.55% by weight, with an average of 1.39%. X-ray diffraction analysis reveals a significant presence of clay, primarily in the form of montmorillonite (Latif et al., 2022). The total alkali content in the samples is remarkably low, ranging from 0.03% to 0.98% by weight. The analyzed samples exhibit a low MgO content, varying from 0.06% to 0.46% by weight, with an average of 0.27%. The samples exhibit high Fe_2O_3 content, ranging from 0.5% to 15% by weight, with an average of 4.29%. The maximum Fe_2O_3 concentrations are found in the massive types of manganese deposits and jasperite. The analyzed samples from the Sulaimani metallogenic province display a wide range of MnO content, varying from 4.9% to 23.9% by weight, with an average of 11.52%. Notably, higher concentrations of MnO have been found in the vein types of deposits, with the maximum reaching 24% and the lowest in the metalliferous Umber unit. The concentration of TiO_2 in all samples is relatively low, with values less than 0.5% by weight, and in some cases, it is even less than 0.01%. The concentration of P_2O_5 in all samples is relatively low, being less than 0.12% by weight. The concentration of BaO in the samples is relatively low but higher compared to other oxides like P_2O_5 and TiO_2, ranging from 0.1% to 1.09% by weight. The highest concentration of BaO is recorded in the massive types of manganese deposits. This high concentration indicates the presence of mineral barite in the massive deposits, which reflects a substantial contribution of oceanic water to the formation of these deposits. In the manganese deposit samples, the compatible trace elements comprise Ni, Co, Cr, V, and Cu. The concentrations of these elements vary in different types of manganese mineralization within the studied area. The highest values of Cr and Co are recorded in vein types of manganese deposits, while the highest concentrations of Ni, Zn, and V are found in massive types. In the studied area, the concentrations of Large-Ion lithophile element (LILE) vary across different types of manganese deposits. The highest values of LILEs are recorded in veins and banded types of manganese deposits, while the lowest concentrations are found in massive types.

In the studied samples High field strength elements (HFSE) include Ti^{4+}, Zr^{4+}, Nb^{5+}, Ta^{5+}, and Hf^{4+}. The concentration behavior of HFSE relative to LILEs is exactly opposite, with the highest HFSE concentrations. found in the massive types of manganese deposits. This difference in behavior can be attributed to the distinct geochemical properties of HFSE, leading to their unique distribution patterns in the different types of manganese deposits.

The total rare earth elements content is very low (10.3 to 80 ppm), with a maximum of 80 ppm observed in the vein type and the lowest concentration of 10.39 ppm in the massive types of manganese deposits (Table2.). The chondrite normalized REE patterns generally exhibit flat profiles, with negative anomalies for both Ce (-0.016 _ -1.024) and Eu (0.54 _ 0.71) observed in most of the samples (Fig. 3A). Moreover, when the REE patterns are normalized to the composition of Post-Archean Australian Shale (PAAS), the samples show similar patterns with Y positive anomalies, except that the intensity of the Eu negative anomaly is reduced (Fig. 3B).

6. Discussion

6.1 Elemental associations and their geochemical clue

6.1.1 Geostatistics: principal component analysis (pca)

There are different types of PCA methods, which include R-mode PCA and Q-mode PCA (Neff, 1994). R-mode PCA primarily focuses on variables (elements in this study) and is suitable for identifying associations between variables

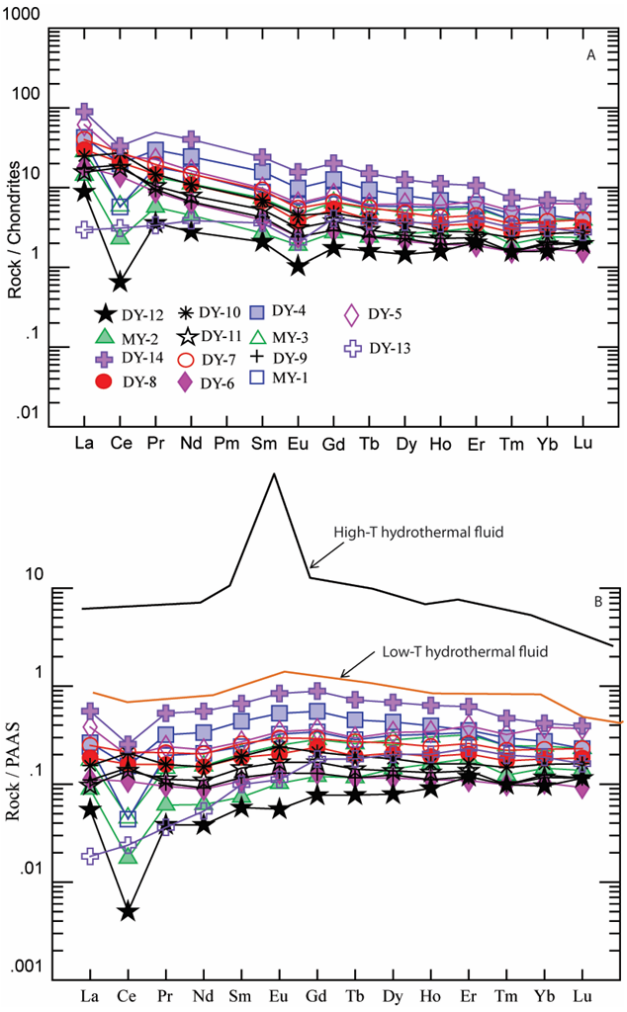

Figure 3. (A) REE patterns in manganese deposit samples from the Sulaimani metallogenic province, normalized to chondrite values as per (Sun and McDonough, 1989) data from 1989. (B) REE patterns in manganese deposit samples from the Sulaimani metallogenic province, normalized to Australian shale values as per (McLennan, 1989). The REE pattern of hydrothermal fluid from both high and low-temperature sources, as reported by (Bau and Dulski, 1999).

and a set of observations. On the other hand, Q-mode PCA is mainly based on observations (samples, not shown in this study) and is used to characterize multivariate observations and understand patterns among them. Principal Component Analysis enables the identification of correlated element clusters (Neff, 1994). The principal component and correlation matrices have been performed using the GEOstats Excel sheet (Gunduz and Asan, 2022). The initial four principal components (PCs) encompass a significant portion of the variances, reaching up to 93%. Notably, PC1, PC2, and PC3 encompass 83.6% of the total variability in the entire geochemical dataset. The principal component PC1 (Fig. 4) explains 67.63% of the total eigenvalues and primarily demonstrates an anticorrelation between Fe and Mn. As a result, this axis closely aligns with the Fe-Mn side of the (Bonatti et al., 1972) triangle.

After plotting the first three principal components (PCs) on the two biplots (Figs. 4 A & B), distinct patterns emerge. SiO_2 stands apart from other elements (Figs. 4 A & B), exhibiting anomaly conditions, which reflect chert influence (Latif et al., 2022). Additionally, the biplots of PC1 and PC2 versus PC3 reveal a strong correlation between REEs and major oxides like Al_2O_3, Na_2O, and K_2O, suggesting that REEs are predominantly associated and hosted with clay minerals and phosphates within the studied manganese deposit rather than the manganese phases. Furthermore, a high correlation is observed between Fe and As, as well as between CaO and V, which likely indicates their association with hematite and carbonate, respectively, both of which are abundant in some rock samples. Moreover, MnO displays notable correlations with Ga, Ba, P_2O_5, U, and Sr, suggesting that these elements are hosted in manganese and

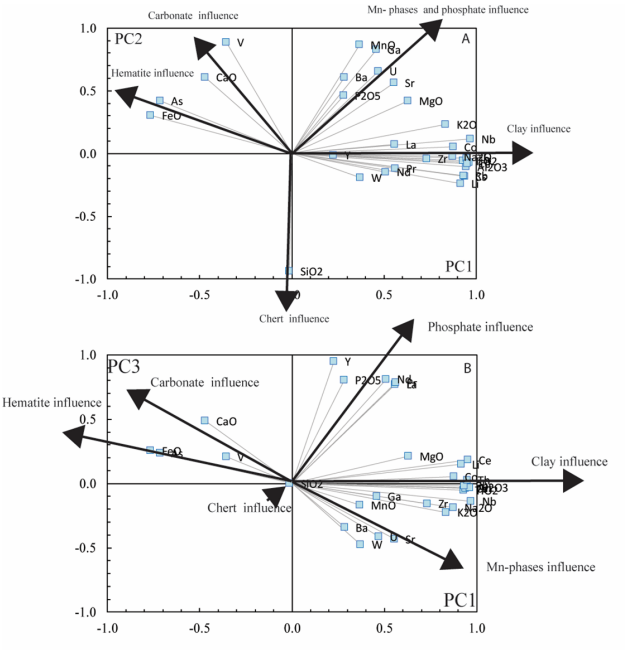

Figure 4. A biplot graph displaying (A) Principal Component 1 (PC1) versus Principal Component 2 (PC2) for the Manganese dataset from the Sulaimani metallogenic provinces, (B) Principal Component 1 (PC1) versus Principal Component 3 (PC3) for the Manganese dataset from the Sulaimani metallogenic provinces. An arrow is used to indicate enrichment along this direction, in addition to the expected phase control.

phosphate phases within the deposit. The positive correlation with K_2O may imply the potential presence of MgO within the montmorillonite crystal structure.

6.1.2 Geostatic: correlations coefficient

A lack of notable positive correlation between SiO_2 and other primary elements may indicating that SiO_2 predominantly occurs as microcrystalline quartz. This quartz is observed in the form of chert within the studied region. The elevated concentration of CaO can be ascribed to the presence of authigenic calcium. This calcium is liberated during the serpentinization process of pyroxene and subsequently deposited as calcium carbonate in the extensive manganese ore characteristic of the surveyed area (. Moreover, a conspicuous positive relationship is apparent with alkali elements, specifically Na_2O and K_2O, suggesting their probable simultaneous occurrence within distinct mineral phases, probably in clay mineral. The limited presence of alkali elements suggests a minor impact from detrital phases rich in Na and K, like plagioclase and pyroxene. This observation could imply that the deposition setting was far from continental edges and their material contribution. Additionally, this might indicate that the source rock for manganese is deficient in alkali elements, resembling more ultramafic rock compositions. The lack of a distinct correlation with other significant oxide components suggests that MnO likely exists as an independent phase within the analyzed specimens. This observation is reinforced by X-ray diffraction data from (Latif et al., 2022), which indicates a straightforward composition of manganese minerals primarily comprised of MnO. The evident positive correlation between CaO and Fe_2O_3 suggests that iron may be incorporated into the crystal structure of carbonate minerals as a siderite component. The absence of a clear relationship with other major oxides suggests that MnO occurs as a separate phase in the studied samples. This observation is further supported by XRD data (Latif et al., 2022), which indicates that manganese mineral composition is simple, consisting mainly of MnO. Indeed, the observation of a very strong positive correlation between MnO and Ga in the samples suggests a significant relationship between these elements. This correlation could imply that gallium is predominantly hosted within the manganese phases present in the samples. It indicates that there might be a close association between gallium and manganese minerals, and the presence of manganese phases may contribute to the accumulation or incorporation of gallium in the studied samples. The notable strong correlation between TiO_2 and Al_2O_3 implies that TiO_2 might be incorporated into the crystal structure of clay minerals. The weak positive correlation between CaO and P_2O_5 indicates that there is very little contribution of phosphate minerals associated with the Mn-bearing ore. The elevated content of BaO points toward the existence of the mineral barite
within the massive deposits. This presence suggests a significant involvement of oceanic water in the process of forming these deposits. The significant presence of Ni (with values exceeding 100 ppm) may suggest contributions from mafic-ultramafic rocks in the source rocks of manganese deposits,

especially in the massive type. The positive correlation among Zn, V, and Ni indicates cogenetic geochemical behaviors among these elements. This correlation suggests that they have a shared origin and may have been deposited together during the formation of the manganese deposits in the studied area. LILEs are considered low ionic potential elements, which means they tend to readily form inner sphere aqua complexes in aqueous solutions. These elements are relatively large enough to be surrounded and coordinated by water molecules, making them more soluble in aqueous solutions (Lee, 2018). As a result, LILEs are likely to be transported away from the mid-oceanic ridge (MOR) axis and reside farther from it. The low contents of LILEs in the manganese deposits may be attributed to the original nature of the manganese-producing reservoir, which is believed to be associated with the ultramafic unit of ophiolite. This suggests that the source rocks for manganese in this area were rich in ferromagnesian minerals, which influenced the abundance of LILEs in the deposits. However, a majority of the samples exhibit distinct negative Ce anomalies, indicating the influence of oceanic water. On the other hand, samples displaying slight positive Ce anomalies might be linked to subsequent diagenetic alterations impacting these particular samples. This suggests the possibility of certain diagenetic activities occurring after the initial deposition of these samples. The consistent and uniform REE and PAAS pattern observed among various types of manganese ore in the study area strongly suggests a cogenetic origin of the deposits. When the REE patterns remain similar across different types of manganese deposits, it indicates that these deposits likely share a common source of origin.

6.2 Paleo redox

In the study area, the Mn/Fe ratio in the Mn deposit ranges from 0.01 to 25.69. This range indicates significant variability in the relative concentrations of manganese (Mn) and iron (Fe) in the deposit. A Jasperite rock with Mn/Fe ratio of 0.01 suggests that the deposit is rich in iron compared to manganese. This may indicate reducing conditions in the environment during the formation of the jasperite, as iron tends to be more stable in its reduced form under such conditions (Lepp, 1963). A Mn/Fe ratio of 25.69 in vein types indicates that the deposit is abundant in manganese compared to iron. This may suggest oxidizing conditions in the environment during the deposit formation, as manganese is more stable in its oxidized form under such conditions (Lepp, 1963). The wide range of Mn/Fe ratios (from 0.01 to 25.69) suggests that the redox conditions in the study area might have varied significantly during the formation of the manganese deposit in Sulaimani metallogenic deposit. This variability could be due to various factors, such as changes in the availability of oxygen, and distance from the manganese discharge sources. The immobile trace elements Co/Ni ratio of 0.34 in the studied manganese samples indicates a reduced environment, further supporting the inference that the manganese deposit is associated with a hydrothermal setting. Reduced environments are commonly observed in hydrothermal systems where hot, mineral-rich fluids interact with surrounding rocks, dissolving, and transporting metals like cobalt and nickel (Pirajno, 2009; Barnes, 1997). The samples with Th/U ratio of less than 1 typically suggest a reducing or anoxic environment (Krishnaswami and Lal, 1978). While samples with Th/U ratio of more than 1 often suggest an oxidizing or oxic environment (Krishnaswami and Lal, 1978). This variability in Th/U ratio may indicate that the depositional environment likely underwent transitions between oxic and anoxic conditions during the formation of the manganese deposit in the study area. The range of Ce_{anom} values in the studied samples from -0.7 to 0.12 confirms the oxic to anoxic nature of the Neotethys oceanic basin during the deposition of manganese. The presence of both negative and positive Ce anomalies within this range suggests fluctuations in the redox conditions in the ocean water during sedimentation (German and Elderfield, 1990). This variation can be associated with changes in oxygen levels, cyclic nature of the manganese bearing hydrothermal fluid and organic matter deposition factors influencing the redox state of the environment.

6.3 Genesis of the manganese deposit in the study area

Based on the trace elements geochemical data and the positioning of the ore samples within or close to the hydrothermal field in the ternary diagrams (Fe-Mn-(Ni + Cu + Co) *10 and 5(Cu + Ni)-100*(Zr + Y + Ce)-((Fe + Mn)/4), it is reasonable to classify the manganese ore in the study area as a hydrothermal type manganese ore deposit (Figs. 5A & B).

The Co/Zn ratios in the analyzed samples vary from 0.01 to

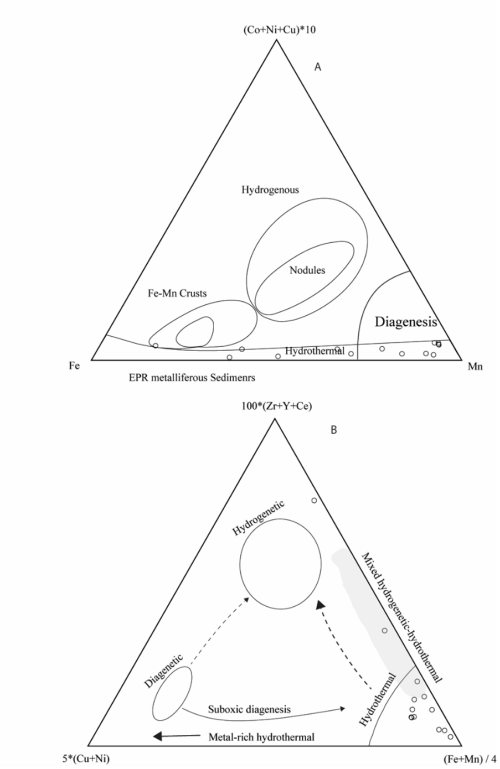

Figure 5. A ternary manganese discrimination based on (A) (Cu + Ni + Co) * 10 - Fe – Mn) (after Bonatti et al. (1972) and later refined by Crerar et al. (1982), (B) (Fe+Mn)/4 - 5*(Cu+Ni) - 100*(Zr+Y+Ce) (after (Josso et al., 2017). It is used to categorize and differentiate manganese occurrences in Sulaimani metallognic district.

2.22, with an average of 0.94. Hydrothermal Mn deposits typically have Co/Zn ratios around 0.15, whereas hydrogenous Mn deposits have Co/Zn ratios higher than 2.5 (Usui et al., 2017). Comparing the average Co/Zn ratio of 0.94 in the studied samples to the values seen in hydrothermal Mn deposits, it falls within the range typical for hydrothermal deposits. This suggests that the Mn deposit in the study area is primarily linked with hydrothermal activity, despite late minor diagenetic overprint. The presence of ore samples within or near the hydrothermal field on these ternary diagrams suggests that the manganese mineralization in the study area is likely associated with hydrothermal activity. Hydrothermal deposits are formed through the interaction of hot, mineral-rich fluids with the surrounding rocks serpentinite parent rocks in the study area along the paleo MOR. These fluids are typically derived from oceanic sources circulating through fractures and faults along a ridge axis. In a hydrothermal setting, as the hot fluids come into contact with the host rocks, they dissolve and carry away various elements, including Mn, Ni, Cu, Co, Zn, and other trace elements. When these fluids cool down by seawater, they precipitate out minerals, leading to the formation of manganese ore deposits (Morgan, 2005). The REE contents in the manganese deposit in the study area range from 6.04 to 80.82 ppm, with an average of 30.13 ppm across all samples. The data suggest that the total REE of the studied deposit is relatively low. This means that the concentration of rare earth elements in the manganese deposit is not as high as those found in some other types of deposits, particularly hydrogenous deposits. The REE pattern of the samples from the Mn deposit in the study area corresponds to that of hydrothermal deposits. Hydrothermal Mn-oxides typically exhibit modest REE compositions, with total REE content around 100 ppm. This pattern is in contrast to hydrogenous deposits, where the total REE content is significantly higher, often exceeding 1000 ppm (Bau et al., 2014). Moreover, the biplot of Ce_{sn}/Ce^{*}_{sn} vs. Y_{sn}/Ho_{sn} show that all studied samples plot in the field of hydrothermal-type Mn deposits (Bau et al., 2014) (Fig. 6A). Overall, the geochemical data and analyses suggest that the manganese deposit in the study area is characterized by relatively low total REE content and exhibits geochemical signatures consistent with hydrothermal-type Manganese deposits.

6.4 Nature of hydrothermal fluid

When hydrothermal fluids are generated through high-temperature processes, they exhibit a pronounced positive europium anomaly (Michard, 1989; Bau and Dulski, 1999). The positive Eu anomaly indicates that europium is preferentially mobilized and enriched in the hydrothermal fluids under these conditions. This phenomenon has been observed and studied in various geological settings encompasses high-temperature hydrothermal fluid (Bau and Dulski, 1999). In contrast, hydrothermal fluids produced by low-temperature hydrothermal alteration do not show a significant Eu anomaly or may not have one at all (Bau and Dulski, 1999). The absence or weak expression of the Eu

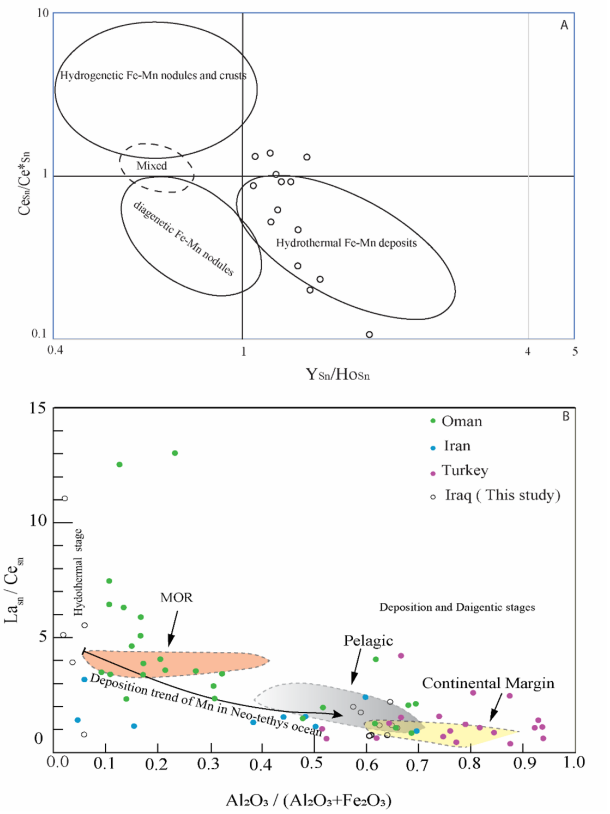

Figure 6. (A) REE based manganese discrimination diagram Ce_{SN}/Ce_{SN*} vs. Y_{SN}/Ho_{SN}, as presented by Bau et al. (2014), provide supporting evidence for the hydrothermal origin of manganese deposits found in the Sulaimani metallogenic deposit. B) La_n/Ce_n vs. $Al_2O_3 / (Al_2O_3 + Fe_2O_3)$, tectonic discrimination diagram for manganese ores in the Zagros region. Normalizing values are from (Evensen et al., 1978). the data source for Oman, Iran, and Turkey area explained elsewhere in the text.

anomaly in these fluids is characteristic of the geochemical processes taking place at lower temperatures in addition to lack of plagioclase in the source. The absence of sharp positive europium anomalies in the geochemical signature of the manganese deposits in the study area confirms the involvement of low-temperature hydrothermal fluids in their formation (Fig. 6B).

6.5 Proposed model for the mn^{2+} source in the area and tectonic setting

(Chen et al. (2018) and reference there in) propose a variety of potential sources for manganese (Mn) deposits. These sources include seawater, hydrothermal-exhalative processes, exhalative-terrigenous inputs, lower crust/mantle contributions, volcanic ash, and oceanic magmato-sedimentary sources. Since serpentinized harzburgite is the predominant altered rock in the study area, this study ultimately suggests that the Mn, Fe and other metals in the area are primarily derived from ultramafic rocks through a serpentinization process. Moreover, the low total rare earth elements and alkali elements, combined with elevated Ni contents in the manganese deposit in the area, support the idea that ultramafic rock could be the best candidate for the parent material.

Low total REE in addition and alkali elements in addition to elevated Ni contents in managnese deposit in the area

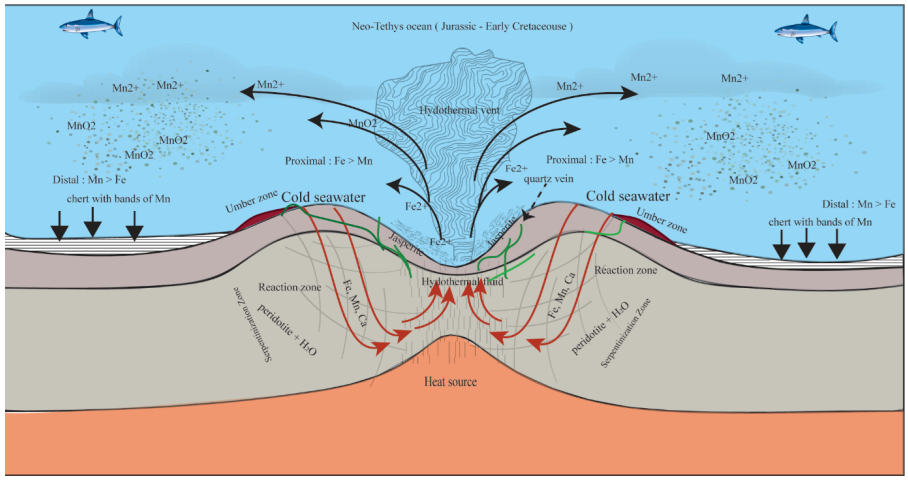

Figure 7. A proposed model after Latif et al. (2022), explaining the genesis of manganese deposits linked to Neotethys radiolarite involves the infiltration of cold deep seawater through fractures in a weakened zone along the Mid-Ocean Ridge (MOR) reaction zone within the crust-upper mantle segment of the Neotethys oceanic crust.

in support for ultramafic rock to be a best candidate. During serpentinization, water interacts with ultramafic rocks (Fig. 7), which are rich in magnesium and iron. This interaction leads to the formation of serpentine minerals and the release of various elements, including Mn, Fe and other metals. The proposed model describes the occurrence of an ultramafic harzburgite body in a mid-oceanic ridge setting within the Penjween ophiolite. The upper mantle unit of the ophiolite undergoes varying degrees of serpentinization due to the infiltration of deep seawater through fractures in the oceanic crust before obduction (Mohammad, 2011). In the reaction zone, the infiltrated seawater reacts with the ultramafic rocks, leading to the formation of syn serpentinization fluid enriched in Fe, Mn, Ca, and Mg (Mohammad, 2011) via leaching. This heated fluid becomes buoyant and is rapidly discharged to the ocean floor through plumes and vents or by infiltrating through additional fractures. Mixing with seawater results in the formation of diffuse hydrothermal fluid enriched in Mn and Fe. The proposed model aligns with previous research findings. Mineral chemistry data obtained from meta harzburgite of the Penjween ophiolite reveals the manganese content in the parent minerals. The original olivine contains up to 0.4 wt. % MnO, while the chromian spinel contains up to 1.2 wt. % MnO (Mohammad, 2011). During the hydrothermal alteration process, the parent minerals undergo transformation into new minerals. The chromium magnetite and serpentine formed from the alteration of olivine and chromian spinel, respectively, exhibit decreasing MnO content. The chromium magnetite contains about 0.1 wt. % MnO, and the serpentine contains about 0.25 wt. % MnO (Mohammad, 2011). Combining rare earth element (REE) data with the $Al_2O_3/ (Al_2O_3 + Fe_2O_3)$ ratios provides a useful method to determine the depositional tectonic environment of manganese ores, as demonstrated by Xie et al. (2013) using a L_{sn}/C_{sn} vs. $Al_2O_3/ (Al_2O_3 + Fe_2O_3)$ tectonic discrimination plot (Fig. 5B) (Murray, 1994).

In the context of the Zagros manganese deposits, the samples fall within a specific range on the discrimination plot, spanning between fields associated with spreading ridge proximal manganese deposits and a distal pelagic field to a continental margin. This suggests that most of the manganese deposits along the Zagros orogeny likely originated from a proximal-distal hydrothermal source with the Neotethys oceanic basin. Furthermore, this finding supports the idea that all manganese deposits associated with radiolarite chert facies, from Oman to Turkey, are linked to regional mid-oceanic ridge hydrothermal activity within Neotethys rather than local volcanic activity. The geochemical data from Oman, Turkey, and Iran are (Robertson and Fleet, 1986; Ozturk, 1997; Oksuz, 2011; Zarasvandi et al., 2013; Zarasvandi et al., 2016).

6.6 Manganese nodules problem in the area

Manganese nodules are deposits that form in situ (authigenic) and through diagenesis (diagenetic) (Hein, 2016; Usui et al., 1993; Cronan, 1977). They mainly consist of manganese oxides and contain significant amounts of Fe, Co, REE, Ni, and Cu. These nodules are distributed throughout all the oceans worldwide, but they are typically found in regions characterized by slow sediment accumulation and a wide ocean floor. There are two primary types of manganese nodules: hydrogenous, which originate from seawater, and diagenetic, which are the result of redox reactions occurring during sediment diagenesis. The formation of manganese nodules is relatively straightforward, involving the precipitation of metal compounds dissolved in seawater around a nucleus on the ocean floor. This growth can occur in two ways: hydrogenous growth happens near the sediment-water interface as metal compounds sink and precipitate, while diagenetic growth occurs within the sediments themselves through the remobilization and reprecipitation of manganese along faults and low-strain zones with high porosity and permeability in the host rock. These two types of nodules, hydrogenous and diagenetic, exhibit distinct differences in their geochemical composition and internal structure. Hydrogenous nodules show well-developed internal layering around nuclei and contain higher levels of Cr, Cu, Ni, and total rare earth elements with a positive cerium anomaly. On the other

hand, diagenetic nodules lack complex internal structures, have lower levels of Cr, Cu, Ni, and total REE, and generally display weak negative cerium anomalies (Fig. 8). By integrating petrographic analysis with the rare earth element pattern, it is possible to propose that the manganese macro-nodule in the study area is of diagenetic origin.

Throughout the diagenetic alterations of the manganese-rich beds containing chert, ore minerals were remobilized during deformation events, leading to the formation of centimeter-scale nodules of pyrolusite. Additionally, the presence of rhythmic alternations between quartz-rich chert beds and clay-rich interbeds, around the manganese rich layer indicates a significant differential diagenetic modification of the radiolarite chert in the studied region (Abrajevitch, 2020).

6.7 Eh-pH diagram and mechanism of fe-mn-si depositions in neotethys.

To identify the paleo-oceanography and depositional settings of Fe-Mn-Si elements that are released via hydrothermal solutions along the Neotethys ridge axis, an Eh-pH diagram can serve as a useful tool (Figs. 9 A & B) (Glasby and Schulz, 1999). This diagram helps trace the formation and stability of the expected Fe-Mn-Si phases in the Neotethys oceanic basin as follow:

Serpentinization is a widespread geochemical process where peridotite undergoes aqueous alteration to transform into serpentine minerals along the MOR (Kelley et al., 2001; Fruh-Green et al., 2004). The fluid produced during serpentinization is characterized by relatively high pH levels (ranging from 10.9 to 12) and low concentrations of Si, Mg, Fe, and Mn, while having high concentrations of Na, K, Ca, and Cl^- (Charlou et al., 2002; Kelley et al., 2001)

As the fluid is released along the vents in the mid-ocean ridge axis, the Fe components of the fluid react with the low oxygen content of the ocean bottom environments, under low Eh (oxidation-reduction potential) conditions around -0.2 V. This leads to the formation of hematite (Fig. 9A), as hematite tends to favor less oxidized environments.

At the same time, manganese occurs as Mn ions in hydrothermal fluid. When the high pH hydrothermal fluid mixes with the moderate pH conditions of the ocean (pH 7.9, Fig. 9D), it undergoes a shift to a lower pH solution (pH 7-8). This shift is a result of homogenization processes occurring near the ocean bottom. As a consequence, silica (SiO_2) is deposited in the form of jasper or microcrystalline quartz (Fig. 9C). This deposition can lead to the formation of jasperite near the discharge area. In the studied area, the co-occurrence of hematite and quartz in the form of jasperite can be observed, either as patches in metabasalt or as layers above basaltic rocks. On the Eh-pH diagram (Fig. 9B), the formation of Mn-minerals (manganese deposits) can follow two possible scenarios and paths:

Scenario 1: Under conditions of low Eh (low oxygen) and high pH, as indicated on the Eh-pH diagram (Fig. 9B), the first manganese (Mn) mineral to form will be manganite among the manganese phases. It is likely and expected to be found in association with hematite or close to the location

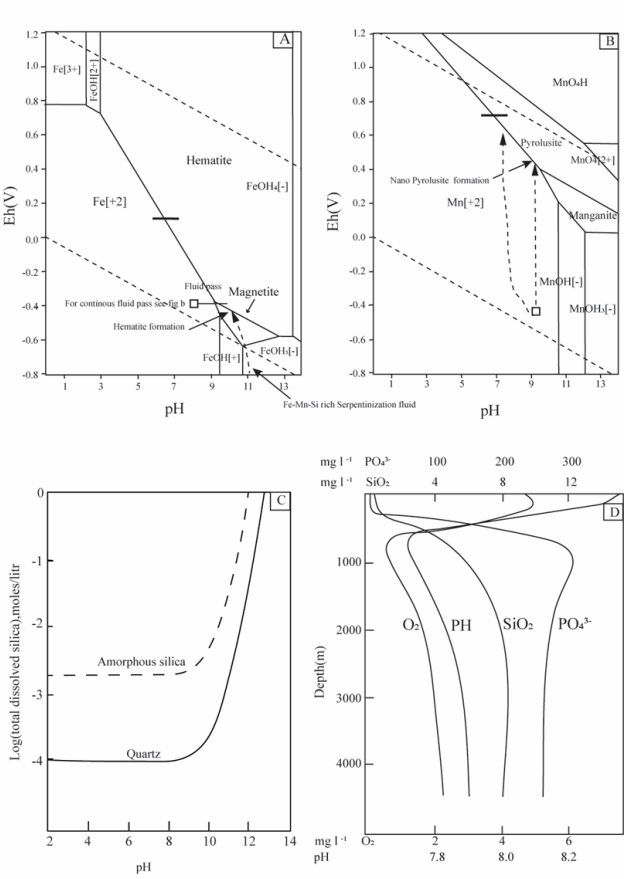

Figure 9. Manganese and iron precipitation mechanism to form various phases in the study area (A) Eh-pH stability diagram for Fe (B) Eh-pH stability diagram for Mn species (Diagrams after (Brookins, 1988; Force and Cannon, 1988), (C) Solubility of SiO_2 vs. pH calculated from thermodynamic value given by (Weast et al., 1986) (D) SiO_2, PO_4, O_2 and pH profile of oceanic water column (Schlesinger and Bernhardt, 2013). The precipitation trend of hematite and pyrolusite shown on Fig. 8 A & B.

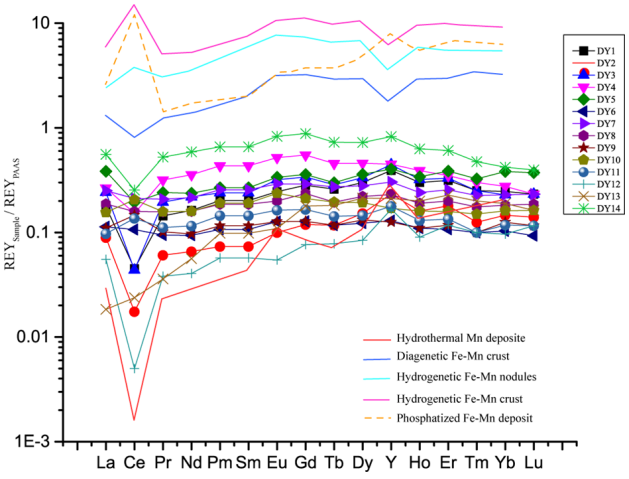

Figure 8. REY_{SN} patterns of various manganese deposit types in the Sulaimani metallogenic deposits, juxtaposed with patterns from marine hydrothermal Fe and Mn deposits, diagenetic Fe-Mn nodules, hydrogenetic Fe-Mn nodules, hydrogenetic Fe-Mn crusts, phosphatized hydrogenetic Fe-Mn crusts. The data for this comparison is sourced from Bau et al. (1996), with values normalized according to McLennan (1989). These patterns are used to analyze and differentiate the geochemical characteristics of manganese deposits in the Sulaimani region in comparison to other types of deposits.

where hematite has been deposited. Over time, through the process of diagenesis and oxidation, manganite will undergo solid-state oxidation and be converted into pyrolusite (Dupont and Donne, 2014).

Scenario 2: In environments with high Eh (moderate to highly oxidized conditions) and low pH, to form manganese dioxide in the form of pyrolusite, the aqueous environment requires oxidation (e.g., Eh $>$ 0.5 V at pH $\sim$ 8). The possible oxidants in oceanic water include molecular oxygen, ozone, nitrates, and perchlorate acids. These oxidants can be produced through photochemical processes (Noda et al., 2019). However, these oxidants are generally low in concentration near the ocean bottom. As a result, the likelihood of pyrolusite deposition near the ocean bottom, particularly close to the fluid discharge site, is low. Due to the slow settling time of Mn in solution (Lupton et al., 1980), it tends to rise from the discharging area at the bottom of the oceanic water. As it ascends, it becomes enriched in the rising plume active area in the ocean, above the ocean bottom. Eventually, it reaches a certain oxidized zone in the water column, where it reacts with oxygen to form MnO nuclei.

The nucleation process of the MnO nuclei may lead to the formation of pyrolusite nanoparticles (Graca et al., 2018). This occurs far from the discharge area, in the oxidizing ocean zone. These pyrolusite nanoparticles, due to their small size, remain suspended in the water column for some time. However, eventually, they precipitate due to gravitational forces and settle as nanoparticles on the ocean bottom, away from the ridge axis (Yucel et al., 2011; Gonzalez-Santana et al., 2020). This settling and precipitation of pyrolusite nanoparticles on the ocean bottom led to the development of bands or layers rich in pyrolusite. These bands form at a distance from the ridge axis, where the nanoparticles have settled and accumulated over time. The absence of any preexisting manganite as relict or patches, along with the difficulty of preserving the high pH of serpentinization fluid due to mixing with low pH oceanic water and silica deposition (Figs. 9 C & D), leads to the conclusion that the first scenario is less likely to be the dominant depositional process of manganese formation in Neotethys ocean basin. Instead, this study favors the second scenario as the dominant process of manganese formation in the area, especially near Kani Safi village. The presence of pyrolusite in nano-particle form, as reflected in the banding nature of manganese deposits in the study area, supports the idea that the manganese was formed through the second scenario. The formation of pyrolusite nanoparticles far from the hydrothermal fluid discharge area, within the oxidizing ocean zone, and their subsequent precipitation on the ocean bottom, explains the observed distribution and characteristics of the manganese deposits in the Sulaimani metallogenic deposit as a part of Neotethys ocean basin.

The cyclic nature of hydrothermal vents along the mid-ocean ridge (MOR) results in a continuous variation of Eh-pH conditions in the depositional environment (Haymon et al., 1993; German et al., 1996). This dynamic environment may contribute to the formation of successive layers containing pyrolusite-rich and pyrolusite-free sections. Such cyclic patterns in the form of layered (laminae) type manganese deposit have been observed not only in the study area but also in other parts of the manganese deposit with the Neotethys oceanic basin (Maghfouri et al., 2019). As hydrothermal fluids are periodically released from the vents, they interact with the surrounding oceanic water, leading to fluctuations in the redox potential (Eh) and pH levels. These changes influence the mineral formation processes, including the precipitation and deposition of manganese minerals like pyrolusite. Consequently, the manganese-rich layers are formed during periods of favorable conditions for pyrolusite nucleation and growth, while pyrolusite-free layers may occur when the conditions are not suitable for its formation. Moreover, these cyclic nature hydrothermal vents highlight the significance of the hydrothermal vent activity in shaping the manganese deposition and mineralogical characteristics in the area.

7. Conclusions

The presence of various modes of occurrence and the syngenetic and diagenetic origins suggest a complex geological history and a combination of processes contributing to the formation of manganese deposits in the Sulaimani metallogenic province. The multi-trace and REE discriminations signature, coupled with a REE chondrite normalized pattern observed in the majority of samples, indicates that submarine hydrothermal processes have likely played a significant role in the deposition of the Fe-Mn belt in the study area. The compilation of geochemical data from diverse manganese deposits linked to the Neotethys radiolarite chert facies, spanning from Oman to Turkey, indicates a predominant association with hydrothermal activity along mid-oceanic ridges. This suggests that these deposits are likely connected to such ridge-related processes rather than being influenced by alternative tectonic settings or genetic processes. The deposition of manganese, iron, and silica within the Neotethys oceanic basin is primarily controlled by the Eh-pH conditions. These conditions play a significant role in influencing the precipitation and accumulation of these elements. The cyclic activity of hydrothermal vents along the mid-oceanic ridges further contributes to the continuous variation in Eh-pH conditions in the depositional environment. The close association of serpentinite and radiolarite bearing manganese deposits may verify a temporary and spatial relationship between these two types of rocks. The serpentinization of ultramafic units and subsequent hydrothermal alteration played a crucial role in providing a significant source of manganese and silica, contributing to the formation of manganese deposits in the studied area and the entire radiolarite facies within the Neotethys realm.

Acknowledgment:

The authors are very grateful to Dr. N. Daneshvar from Kurdistan University, Iran are highly appreciated for their fruitful discussions and help. Thank you to the four anonymous reviewers for their invaluable feedback and insightful comments, which have improved the quality of this work. Special appreciation goes to Editor-in-Chief Dr. Rahim Dabri for his invaluable guidance in overseeing the paper and providing insightful advice on the early versions.

Authors contributions
Authors have contributed equally in preparing and writing the manuscript.

Availability of data and materials
The data that support the findings of this study are available from the corresponding author, upon reasonable request.

Conflict of interests
The authors declare that they have no conflicts of interest.

References

Abrajevitch A. (2020) Diagenetic formation of bedded chert: implications from a rock magnetic study of siliceous precursor sediments. *Earth and Planetary Science Letters* 533:116039. DOI: https://doi.org/10.1016/j.epsl.2019.116039.

Al-Bassam K. S. (1984) Final report on the regional geological survey of iraq. *Economic Geology of Iraq* 5 DOI: https://doi.org/http://87.98.241.163/Xmlui/Handle/123456789/32160.

——— (2013) Mineral resources of kurdistan region, iraq. *Iraqi Bulletin Of Geology And Mining* 9:103–127. DOI: https://doi.org/https://ibgm-iq.org/ibgm/index.php/ibgm/article/view/241.

Aydogan M. S. (2021) An example of ridge-proximal hydrothermal mineralization: evidence from radiolarian chert-hosted fe-mn-oxide mineralization within the izmir-ankara-erzincan neotethyan ocean, central turkey. *All Earth* 33:136–160. DOI: https://doi.org/10.1080/27669645.2021.2003009.

Barnes H. L. (1997) Geochemistry of hydrothermal ore deposits. *John Wiley & Sons, United States of America.*

Bau M., Dulski P. (1999) Comparing yttrium and rare earths in hydrothermal fluids from the mid-atlantic ridge: implications for y and ree behaviour during near-vent mixing and for the y/ho ratio of proterozoic seawater. *Chemical Geology* 155:77–90. DOI: https://doi.org/10.1016/S0009-2541(98)00142-9.

Bau M., Koschinsky A., Dulski P., Hein J. R. (1996) Comparison of the partitioning behaviours of yttrium, rare earth elements, and titanium between hydrogenetic marine ferromanganese crusts and seawater. *Geochimica et Cosmochimica Acta* 60 (10): 1709–1725. DOI: https://doi.org/10.1016/0016-7037(96)00063-4.

Bau M., Schmidt K., Koschinsky A., Hein J., Kuhn T., Usui A. (2014) Discriminating between different genetic types of marine ferromanganese crusts and nodules based on rare earth elements and yttrium. *Chemical Geology* 381:1–9. DOI: https://doi.org/10.1016/j.chemgeo.2014.05.004.

Baziany M. M. (2014) Depositional systems and sedimentary basin analysis of the qulqula radiolarian formation of the zagros suture zone, sulaimani area, iraqi kurdistan region. *Unpublished Ph. D. Thesis, university of sulaimani.*

Bonatti E., Fisher D., Joensuu O., Rydell H., Beyth M. (1972) Iron-manganese-barium deposit from the northern afar rift (ethiopia). *Economic Geology* 67:717–730. DOI: https://doi.org/10.2113/gsecongeo.67.6.717.

Brookins D. G. (1988) Eh-ph diagrams for geochemistry. *Springer Berlin Heidelberg.,* DOI: https://doi.org/10.1007/978-3-642-73093-1.

Buday T., Jassim S. Z. (1984) Tectonic map of iraq, scale 1: 1000 000. *Geological Survey and Mineral Investigation.*

Charlou J. L., Donval J. P., Fouquet Y., Jean-Baptiste P., Holm N. (2002) Geochemistry of high h2 and ch4 vent fluids issuing from ultramafic rocks at the rainbow hydrothermal field (36°14′n, mar). *Chemical Geology* 191:345–359. DOI: https://doi.org/10.1016/S0009-2541(02)00134-1.

Chen F., Wang Q., Yang S., Zhang Q., Liu X., Chen J., Carranza E. J. M. (2018) Space-time distribution of manganese ore deposits along the southern margin of the south china block, in the context of palaeo-tethyan evolution. *International Geology Review* 60:72–86. DOI: https://doi.org/10.1080/00206814.2017.1320689.

Crerar D. A., Namson J., Chyi M. S., Williams L., Feigenson M. D. (1982) Manganiferous cherts of the franciscan assemblage; i, general geology, ancient and modern analogues, and implications for hydrothermal convection at oceanic spreading centers. *Economic Geology* 77:519–540. DOI: https://doi.org/10.2113/gsecongeo.77.3.519.

Cronan D. S. (1977) Chapter 2 deep-sea nodules: distribution and geochemistry. in g. p. glasby (ed.). *Elsevier* 15:11–44. DOI: https://doi.org/10.1016/S0422-9894(08)71016-X.

Dabiri R., Hagdoust H., Arjmandzadeh R. (2018) Geochemical distribution of heavy metals and assessment of environmental indicators in chah-shaljami polymetal ore deposit, south of birjand, iran. *Geopersia* 8:307–317. DOI: https://doi.org/10.22059/geope.2018.260186.648395.

Dupont M. F., Donne S. W. (2014) Nucleation and growth of electrodeposited manganese dioxide for electrochemical capacitors. *Electrochimica Acta* 120:219–225. DOI: https://doi.org/10.1016/j.electacta.2013.12.014.

Evensen N. M., Hamilton P. J., O'Nions R. K. (1978) Rare-earth abundances in chondritic meteorites. *Geochimica et Cosmochimica Acta* 42:1199–1212. DOI: https://doi.org/10.1016/0016-7037(78)90114-X.

Force E. R., Cannon W. F. (1988) Depositional model for shallow-marine manganese deposits around black shale basins. *Economic Geology* 83:93–117. DOI: https://doi.org/10.2113/gsecongeo.83.1.93.

Fouad S. F. A. (2012) Western zagros fold – thrust belt, part i: the low folded zone. *Iraqi Bulletin of Geology and Mining* 5:39–62. DOI: https://doi.org/https://ibgmiq.org/ibgm/index.php/ibgm/article/view/222.

Fruh-Green G. L., Connolly J. A., Plas A., Kelley D. S., Grobety B. (2004) Serpentinization of oceanic peridotites: implications for geochemical cycles and biological activity. *The Subseafloor Biosphere at Mid-Ocean Ridges* 144:119–136. DOI: https://doi.org/http://perplex.ethz.ch/papers/frueh-green"˙agu"˙04.pdf.

German C., Klinkhammer G., Rudnicki M. (1996) The rainbow hydrothermal plume, 36°15′n, mar. *Geophysical Research Letters* 23:2979–2982. DOI: https://doi.org/10.1029/96GL02883.

German C. R., Elderfield H. (1990) Application of the ce anomaly as a paleoredox indicator: the ground rules. *Paleoceanography* 5:823–833. DOI: https://doi.org/10.1029/PA005i005p00823.

Ghasempour M. R., Ghazi J. Mehdipour, Biabangard H., Dabiri R. (2014) Petrogenetic evolution of plio-quaternary mafic lavas in nehbandan (east iran). *Iranian Journal of Earth Sciences* 6:133–141.

Glasby G. P., Schulz H. D. (1999) Eh ph diagrams for mn, fe, co, ni, cu and as under seawater conditions: application of two new types of eh ph diagrams to the study of specific problems in marine geochemistry. *Aquatic Geochemistry* 5:227–248. DOI: https://doi.org/10.1023/A:1009663322718.

Gonzalez-Santana D., Planquette H., Cheize M., Whitby H., Gourain A., Holmes T., Guyader V., et al. (2020) Processes driving iron and manganese dispersal from the tag hydrothermal plume (mid-atlantic ridge): results from a geotraces process study. *Frontiers in Marine Science* 7:568. DOI: https://doi.org/10.3389/fmars.2020.00568.

Graca B., Zgrundo A., Zakrzewska D., Rzodkiewicz M., Karczewski J. (2018) Origin and fate of nanoparticles in marine water - preliminary results. *Chemosphere* 206:359–368. DOI: https://doi.org/10.1016/j.chemosphere.2018.05.022.

Gunduz M., Asan K. (2022) Geostats: an excel-based data analysis program applying basic principles of statistics for geological studies. *Earth Science Informatics* 15:705–712. DOI: https://doi.org/10.1007/s12145-021-00710-6.

Haymon R. M., Fornari D. J., Damm K. L. Von, Lilley M. D., Perfit M. R., Edmond J. M., Shanks W. C., et al. (1993) Volcanic eruption of the mid-ocean ridge along the east pacific rise crest at 9°45-52′n: direct submersible observations of seafloor phenomena associated with an eruption event in april, 1991. *Earth and Planetary Science Letters* 119:85–101. DOI: https://doi.org/10.1016/0012-821X(93)90008-W.

Hein J. R. (2016) Manganese nodules. *Encyclopedia of marine geosciences, Dordrecht, the Netherlands: Springer,* 408–412.

Jassim S. Z., Goff J. C. (2006) Geology of iraq. dolin, distributed by geological society of london.

Josso P., Pelleter E., Pourret O., Fouquet Y., Etoubleau J., Cheron S., Bollinger C. (2017) A new discrimination scheme for oceanic ferromanganese deposits using high field strength and rare earth elements. *Ore Geology Reviews* 87:3–15.
DOI: https://doi.org/10.1016/j.oregeorev.2016.09.003.

Kelley D. S., Karson J. A., Blackman D. K., Fruh-Green G. L., Butterfield D. A., Lilley M. D., Olson E. J., et al. (2001) An off-axis hydrothermal vent field near the mid-atlantic ridge at 30° n. *Nature* 412:145–149. DOI: https://doi.org/10.1038/35084000.

Kickmaier W., Peters T. J. (1990) Manganese occurrences in the al hammah range-wahrah formation, oman mountains. *Geological Society, London, Special Publications* 49:239–249.
DOI: https://doi.org/10.1144/GSL.SP.1992.049.01.16.

Krishnaswami S., Lal D. (1978) Radionuclide limnochronology. in a. *Lerman (Ed.), Lakes: Chemistry, Geology, Physics, Springer,* 153–177.
DOI: https://doi.org/10.1007/978-1-4757-1152-3‴6.

Latif D., Mohammad Y., Baziany M. (2022) Mineralogy and origin of the manganese deposit in the sulaimani province, kurdistan region of iraq: insight to serpentinization-induced manganese production scenario. *Iraqi Geological Journal* 55:178–200.
DOI: https://doi.org/10.46717/igj.55.1F.15Ms-2022-06-30.

Lee C. T. (2018) Geochemical classification of elements. in w. m. white (ed.). *Encyclopedia of Geochemistry: A Comprehensive Reference Source on the Chemistry of the Earth,* 545–549.
DOI: https://doi.org/10.1007/978-3-319-39312-4‴255.

Lepp H. (1963) The relation of iron and manganese in sedimentary iron formations. *Economic Geology* 58:515–526.
DOI: https://doi.org/10.2113/gsecongeo.58.4.515.

Lupton J. E., Klinkhammer G. P., Normark W. R., Haymon R., MacDonald K. C., Weiss R. F., Craig H. (1980) Helium-3 and manganese at the 21°n east pacific rise hydrothermal site. *Earth and Planetary Science Letters* 50:115–127.
DOI: https://doi.org/10.1016/0012-821X(80)90123-5.

Maghfouri S., Rastad E., Movahednia M., Lentz D. R., Hosseinzadeh M. Reza, Ye L., Mousivand F. (2019) Metallogeny and temporal–spatial distribution of manganese mineralizations in iran: implications for future exploration. *Ore Geology Reviews* 115:103026.
DOI: https://doi.org/10.1016/j.oregeorev.2019.103026.

Mahdavi M., Dabiri R., Hosseini E. Shah (2015) Magmatic evolution and compositional characteristics of tertiary volcanic rocks associated with the venarch manganese mineralization, sw qom, central iran. *Earth Sciences Research Journal* 19:141–145.

McLennan S. M. (1989) Chapter 7. rare earth elements in sedimentary rocks: influence of provenance and sedimentary processes. in b. r. lipin and g. a. mckay (eds.). *Geochemistry and Mineralogy of Rare Earth Elements,* 169–200.
DOI: https://doi.org/10.1515/9781501509032-010.

Michard A. (1989) Rare earth element systematics in hydrothermal fluids. *Geochimica et Cosmochimica Acta* 53:745–750.
DOI: https://doi.org/10.1016/0016-7037(89)90017-3.

Mohammad Y., Qaradaghi J. (2016) Geochronological and mineral chemical constraints on the age and formation conditions of the leucogranite in the mawat ophiolite, northeastern of iraq: insight to syncsubduction zone granite. *Arabian Journal of Geosciences* 9:1–23.
DOI: https://doi.org/10.1007/s12517-016-2630-4.

Mohammad Y. O. (2020) Cumulate and tectonite dunite from mawat ophiolite, kurdistan region, northeastern iraq: field evidence and mineral chemical constraints. *Iraqi Bulletin of Geology and Mining* 16:15–33.
DOI: https://doi.org/https://www.iasj.net/iasj/download/c643b1055ae357e5.

——— (2011) Serpentinites and their tectonic signature along the northwest zagros thrust zone, kurdistan region, iraq. *Arabian Journal of Geosciences* 4:69–83.
DOI: https://doi.org/10.1007/s12517-009-0080-y.

Mohammad Y. O., Ali S. A., Aziz N. R., Yara I. O., Abdulla K. L. (2021) Comment on "generation and exhumation of granitoid intrusions in the penjween ophiolite complex, nw zagros of the kurdistan region of iraq: implications for the geodynamic evolution of the arabia-eurasia collision zone" by ismail et al., 2020, 376-377, 105714. *Lithos* 390:376–377.
DOI: https://doi.org/10.1016/j.lithos.2020.105915.

Mohammad Y. O., Cornell D. H., Qaradaghi J. H., Mohammad F. O. (2014) Geochemistry and ar–ar muscovite ages of the daraban leucogranite, mawat ophiolite, northeastern iraq: implications for arabia–eurasia continental collision. *Journal of Asian Earth Sciences* 86:151–165.
DOI: https://doi.org/10.1016/j.jseaes.2013.09.029.

Mohammad Y. O., Maekawa H., Lawa F. Ahmmad (2007) Mineralogy and origin of mlakawa albitite from kurdistan region, northeastern iraq. *Geosphere* 3:624–645.
DOI: https://doi.org/https://pubs.geoscienceworld.org/gsa/geosphere/article-abstract/3/6/624/31203.

Mollai H., Dabiri R., Torshizian H., Pe-Piper G., Wang W. E. I. (2021) Upper neoproterozoic garnet-bearing granites in the zeber-kuh region from east central iran micro plate: implications for the magmatic evolution in the northern margin of gondwanaland. *Geologica Carpathica* 72:461–481.
DOI: https://doi.org/10.31577/GeolCarp.72.6.2.

Morgan J. J. (2005) Kinetics of reaction between o2 and mn(ii) species in aqueous solutions. *Geochimica et Cosmochimica Acta* 69:35–48.
DOI: https://doi.org/10.1016/j.gca.2004.06.013.

Mosier D. L., Page N. J. (1988) Descriptive and grade-tonnage models of volcanogenic manganese deposits in oceanic environments: a modification. *US Government Printing Office* 1811:1–28.
DOI: https://doi.org/https://pubs.usgs.gov/bul/b1811/b1811.pdf.

Murray R. W. (1994) Chemical criteria to identify the depositional environment of chert: general principles and applications. *Sedimentary Geology* 90:213–232.
DOI: https://doi.org/10.1016/0037-0738(94)90039-6.

Nazari M., Arian M. A., Solgi A., Zareisahamieh R., Yazdi A. (2023) Geochemistry and tectonomagmatic environment of eocene volcanic rocks in the southeastern region of abhar, nw iran. *Iranian Journal of Earth Sciences* 15:228–247.
DOI: https://doi.org/10.30495/ijes.2023.1956689.1746.

Neff H. (1994) Rq-mode principal components analysis of ceramic compositional data. *Archaeometry* 36:115–130.
DOI: https://doi.org/10.1111/j.1475-4754.1994.tb01068.x.

Noda N., Imamura S., Sekine Y., Kurisu M., Fukushi K., Terada N., Uesugi S., Numako C., Takahashi Y., Hartmann J. (2019) Highly oxidizing aqueous environments on early mars inferred from scavenging pattern of trace metals on manganese oxides. *Journal of Geophysical Research: Planets* 124:1282–1295.
DOI: https://doi.org/10.1029/2018JE005892.

Nutman A., Ali S., Mohammad Y., Jones B. G., Zhang Q. (2022) The early eocene (48 ma) qaladeza trondhjemite formed by wet partial remelting of mafic crust in the arc-related bulfat igneous complex (kurdistan, iraq): constraints on the timing of neotethys closure. *Arabian Journal of Geosciences* 15:679.
DOI: https://doi.org/10.1007/s12517-022-09975-7.

Oksuz N. (2011) Geochemical characteristics of the eymir (sorgun-yozgat) manganese deposit, turkey. *Journal of Rare Earths* 29:287–296.
DOI: https://doi.org/10.1016/S1002-0721(10)60446-.

Ousta S. H., Ashja-Ardalan A., Yazdi A., Dabiri R., Arian M. A. (2024) Petrogenesis and tectonic implications of miocene dikes in the southeast of bam (se iran): constraints on the development of active continental margin. *Geopersia* 14:89–111. DOI: https://doi.org/10.22059/geope.2023.364334.648729.

Ozturk H. (1997) Manganese deposits in turkey: distribution, types and tectonic setting. *Ore Geology Reviews* 12:187–203. DOI: https://doi.org/10.1016/S0169-1368(97)00005-X.

Pirajno F. (2009) Hydrothermal processes associated with meteorite impacts. in. *F. Pirajno (Ed.), Hydrothermal Processes and Mineral Systems,* 1097–1130. DOI: https://doi.org/10.1007/978-1-4020-8613-7"¨11.

Polgari M., Hein J. R., Vigh T., Szabo-Drubina M., Forizs I., Biro L., Muller A., Toth A. L. (2012) Microbial processes and the origin of the urkut manganese deposit, hungary. *Ore Geology Reviews* 47:87–109. DOI: https://doi.org/10.1016/j.oregeorev.2011.10.001.

Robertson A. H. F., Fleet A. J. (1986) Geochemistry and palaeooceanography of metalliferous and pelagic sediments from the late cretaceous oman ophiolite. *Marine and Petroleum Geology* 3:315–337. DOI: https://doi.org/10.1016/0264-8172(86)90036-X.

Schlesinger W. H., Bernhardt E. S. (2013) Biogeochemistry: an analysis of global change. waltham, ma. *Elsevier, Academic Press.*

Sissakian V. (2018) The minerals wealth in the kurdistan region, iraq. *UKH Journal of Science and Engineering* 2:23–36. DOI: https://doi.org/10.25079/ukhjse.v2n2y2018.pp23-36.

Sun W., McDonough W. (1989) Chemical and isotopic systematics of oceanic basalts: implications for mantle composition and processes. in. *Geological Society, London, Special Publications* 42:313–345. DOI: https://doi.org/10.1144/GSL.SP.1989.042.01.19.

Taylor S. R., McLennan S. M. (1985) The continental crust: its composition and evolution. xvi + 312 pp. oxford, london, edinburgh, boston, palo alto, melbourne: blackwell scientific. price 16.80 (paperback). isbn 0 632 01148 3. *Geological Magazine* 122:673–674. DOI: https://doi.org/10.1017/S0016756800032167.

Usui A., Nishi K., Sato H., Nakasato Y., Thornton B., Kashiwabara T., Tokumaru A., et al. (2017) Continuous growth of hydrogenetic ferromanganese crusts since 17 myr ago on takuyo-daigo seamount, nw pacific, at water depths of 800-5500 m. *Ore Geology Reviews* 87:71–87. DOI: https://doi.org/10.1016/j.oregeorev.2016.09.032.

Usui A., Nishimura A., Mita N. (1993) Composition and growth history of surficial and buried manganese nodules in the penrhyn basin, southwestern pacific. *Marine Geology* 114:133–153. DOI: https://doi.org/10.1016/0025-3227(93)90044-V.

Weast R. C., Astle M. J., Beyer W. H. (1986) Crc handbook of chemistry and physics 67th edn. *Boca Raton, FL: Chemical Rubber Company*

Wever P. De, Grissac C. Bourdillon de, Bechennec F. (1988) Permian age from radiolarites of the hawasina nappes, oman mountains. *Geology* 16:912–914. DOI: https://doi.org/10.1130/0091-7613(1988)016$¡$0912:PAFROT$¿$2.3.CO;2.

Xie C., Xu L., Peng T., Chen K., Zhao J. (2013) Leaching process and kinetics of manganese in low-grade manganese ore. *Chinese Journal of Geochemistry* 32 DOI: https://doi.org/10.1007/s11631-013-0625-3.

Yazdi A., Shahhosseini E., Moharami F. (2022) Petrology and tectonomagmatic environment of the volcanic rocks of west torud-iran. *Iranian Journal of Earth Sciences* 14:40–57. DOI: https://doi.org/10.30495/ijes.2022.1929200.1601.

Yucel M., Gartman A., Chan C. S., Luther G. W. (2011) Hydrothermal vents as a kinetically stable source of iron-sulphide-bearing nanoparticles to the ocean. *Nature Geoscience* 4:367–371. DOI: https://doi.org/10.1038/ngeo1148.

Zarasvandi A., Lentz D., Rezaei M., Pourkaseb H. (2013) Genesis of the nasirabad manganese occurrence, fars province, iran: geochemical evidences. *Geochemistry* 73:495–508. DOI: https://doi.org/10.1016/j.chemer.2013.02.003.

Zarasvandi A., Rezaei M., Sadeghi M., Pourkaseb H., Sepahvand M. (2016) Rare-earth element distribution and genesis of manganese ores associated with tethyan ophiolites, iran: a review. *Mineralogical Magazine* 80:127–142. DOI: https://doi.org/10.1180/minmag.2016.080.054.